Deoxynivalenol: a trigger for intestinal integrity breakdown

Peyman Akbari,*,†,1 Saskia Braber,*,1,2 Hendrik Gremmels,‡ Pim J. Koelink,†
Kim A. T. Verheijden,† Johan Garssen,†,§ and Johanna Fink-Gremmels*

*Division of Veterinary Pharmacy, Pharmacology, and Toxicology, and †Division of Pharmacology,
Utrecht Institute for Pharmaceutical Sciences, Faculty of Science, Utrecht University, The
Netherlands; ‡Department of Nephrology and Hypertension, University Medical Center Utrecht,
Utrecht, The Netherlands; and §Nutricia Research, Utrecht, The Netherlands

ABSTRACT   Disintegration of the colonic epithelial
barrier is considered a key event in the initiation and
progression of inflammatory bowel and celiac disease.
As the primary etiology of these diseases remains
unknown, we hypothesized that the trichothecene de-
oxynivalenol (DON), a fungal metabolite found in
grain-based human diets, might be one of the triggers
resulting in an impairment of the intestinal tight junc-
tion network preceding an inflammatory response. Us-
ing horizontal impedance measurements, we demon-
strate that DON disintegrates a human Caco-2 cell
monolayer within <1 h after exposure to concentra-
tions as low as 1.39 µM. This initial trigger is followed
by a decrease in transepithelial resistance and an in-
creased permeability of marker molecules, such as
lucifer yellow and FITC-labeled dextran. In parallel,
the increase in paracellular transport of FITC-dextran
is demonstrated *in vivo* in B6C3F$_1$ mice, challenged
orally with DON. *In vitro* claudin protein levels are
decreased and correlated with a displacement within
the cells *in vitro* and *in vivo*, accompanied by a compen-
satory up-regulation of mRNA levels of claudins and
their binding partner ZO-1. In treated mice, alterations
in villus architecture in the entire intestinal tract resem-
ble the disintegration of the epithelial barrier, a char-
acteristic of chronic inflammatory bowel disease.—
Akbari, P., Braber, S., Gremmels, H., Koelink, P. J.,
Verheijden, K. A. T., Garssen, J., Fink-Gremmels, J.
Deoxynivalenol: a trigger for intestinal integrity break-
down. *FASEB J.* 28, 000–000 (2014). www.fasebj.org

Key Words: Caco-2 cells · TEER · tight junction proteins

THE INTESTINAL EPITHELIAL barrier is essential for the
maintenance of physiological gut functions and serves
as the first line of host defense against potentially
harmful stressors from the environment, such as bacte-
ria and viruses, as well as natural antigens and toxins
occurring in food (1–3). The physical intestinal barrier
is primarily formed by epithelial cells, connected by
tight junctions (TJs), which form an anastomosing
network sealing adjacent epithelial cells near the lumi-
nal surface, thus preventing a paracellular transport of
luminal antigens (4, 5). TJs are composed of transmem-
brane proteins, including occludin (OCLN) and clau-
dins (CLDNs), which form a linear barrier at the
apical-lateral membrane of the cell; peripheral mem-
brane proteins, like zona occludens (ZO) proteins, that
serve as a link between the transmembrane TJ proteins;
and cytosolic and nuclear proteins (6, 7). It is well
accepted that a breakdown of the normally impeccable
epithelial barrier of the intestine results in the devel-
opment of a "leaky" gut. Disintegrated intestinal TJs
allow the paracellular infiltration of luminal antigens
and are considered as a pivotal pathogenic factor in the
onset and promotion of chronic intestinal inflamma-
tions, such as inflammatory bowel disease (IBD) and
celiac disease (8–10). Recent experimental evidence
suggests that certain food contaminants, in particulary
the mycotoxin deoxynivalenol (DON) can impair intes-
tinal barrier functions (11–14) and may be directly
involved in intestinal inflammation (15–17). DON, a
Fusarium metabolite, is among the most frequently
detected contaminants of cereal-based foods, including
breakfast cereals (18–21). Considering this regular
human exposure, the aim of the current study was to
characterize the sequence of events induced by DON
that leads to a compromised intestinal barrier function.
Using human Caco-2 cell monolayers as an *in vitro*
model, we investigated the effect of DON on barrier
integrity following apical and basolateral exposure, the
paracellular transport of marker molecules, and alter-

---

[1] These authors contributed equally to this work.
[2] Correspondence: Utrecht University, Yalelaan 104, 3584
CM Utrecht, The Netherlands. E-mail: s.braber@uu.nl

ations in the expression and cellular distribution of TJ proteins. *In vivo* experiments in male B6C3F$_1$ mice, challenged orally with DON, were conducted to substantiate the *in vitro* findings and to demonstrate the effect of DON exposure on villus architecture. The presented results challenge the hypothesis that nutritional DON exposure and the postulated high concentrations of the toxin in the intestinal lumen are the possible explanation for the observed translocation of luminal pathogens, while at the same time providing convincing evidence that DON acts as a trigger for intestinal integrity breakdown.

MATERIALS AND METHODS

DON solution

Purified DON (D0156; Sigma-Aldrich, St Louis, MO, USA) was dissolved in absolute ethanol (99.9%; J.T. Baker, Deventer, The Netherlands) to prepare a 25 mM stock solution, stored at $-20°C$. Serial dilutions of this stock were prepared in cell culture medium. All other chemicals were of the highest purity available.

In vitro experiments

Caco-2 cell cultures

Human epithelial colorectal adenocarcinoma cells (Caco-2 line, passages 5–19; HTB-37; American Type Culture Collection, Manassas, VA, USA) were cultured in 75-cm^2 culture flasks (Greiner Bio-One, Frickenhausen, Germany) in Dulbecco's modified Eagle's medium (DMEM), containing 25 mM HEPES and 4.5 mg/ml glucose (Life Technologies, Inc., Invitrogen, CA, USA), and supplemented with 10% heat-inactivated fetal calf serum (Life Technologies), 100 U/ml penicillin, 100 µg/ml streptomycin, and 2 mM glutamine (Biocambrex, Verviers, Belgium), and 1% nonessential amino acids (Life Technologies). The cells were maintained in a humidified atmosphere of 95% air and 5% CO$_2$ at 37°C. Medium was refreshed every 2–3 d, and cells were passaged $1\times$/wk. For subculture, the confluent cells were trypsinized using 0.05% trypsin and 0.54 mM EDTA and were diluted in culture medium.

Caco-2 cell monolayers on transwell inserts

All *in vitro* experiments were conducted with Caco-2 cells grown on 0.3-cm^2 high-pore-density polyethylene terephthalate membrane transwell inserts with 0.4-µm pores (Falcon; BD Biosciences, Franklin Lakes, NJ, USA) placed in a 24-well plate, if not otherwise stated. The cells were seeded at a density of 0.3×10^5 cells/insert. The cells were incubated at 37°C in a humidified atmosphere of 95% air and 5% CO$_2$. After 17–19 d of culture, a confluent monolayer was achieved, with a mean transepithelial electrical resistance (TEER) exceeding 400 $\Omega \cdot cm^2$ measured by a Millicell-ERS volt-ohm meter (Millipore, Temecula, CA, USA). Each transwell experiment started when the TEER values reached this plateau.

Lactate dehydrogenase (LDH) assay

Caco-2 cells grown on inserts as described above were exposed to DON (0–37.5 µM) for 24 h, and the cytotoxic effect of DON on the Caco-2 cells was evaluated by measuring LDH leakage. LDH leakage was measured in the culture medium of the apical and basolateral compartments using the Cyto-Tox 96 nonradioactive cytotoxicity assay kit (Promega Corp., Madison, WI, USA), according to manufacturer's instructions.

TEER measurement

Caco-2 cells were grown on inserts as described above. The integrity of the cellular monolayer was evaluated by measuring TEER using a Millicell-ERS volt-ohm meter (Millipore). Mean TEER values for untreated cell monolayers were 435 ± 15 $\Omega \cdot cm^2$. The cells were challenged by adding increasing concentrations of DON (0, 0.05, 0.15, 0.46, 1.39, 4.17, and 12.5 µM) to the apical side, the basolateral side, or both sides. TEER was measured at 0, 2, 4, 8, 12, and 24 h after DON exposure.

Paracellular tracer flux assay

Caco-2 cell monolayers grown on inserts as described above were treated with increasing concentrations of DON in the apical and basolateral compartments for 24 h. Thereafter, membrane-impermeable molecules such as lucifer yellow (LY, molecular mass of 0.457 kDa, 6 µg/ml; Sigma-Aldrich) and two different molecular sizes of fluorescein isothiocyanate (FITC)-dextran (molecular mass of 4 and 40 kDa, respectively, 6 µg/ml; Sigma-Aldrich) were added to the apical compartment for 4 h, and paracellular flux was determined by measuring the fluorescence intensity in the basolateral compartment with a fluorometer (FLUOstar Optima; BMG Labtech, Offenburg, Germany) set at excitation and emission wavelengths of 410 and 520 nm, respectively, for LY, and 485 and 520 nm for FITC-dextran.

Real-time horizontal impedance measurements

The xCelligence system (Roche Applied Science, Mannheim, Germany) was used for dynamic monitoring of epithelial barrier integrity, as described before (22, 23). Briefly, 50 µl of the culture medium was added to 16-well E-plates (Roche Diagnostics, Mannheim, Germany) to obtain background readings of the individual wells. Caco-2 cells were seeded into these plates at a density of 5000 cells/well in 100 µl medium and grown for ~2 d to reach confluence, as indicated by a plateau in impedance signal. Since dome formation (24) may lead to detachment of the Caco-2 cells in this E-plate (not observed in transwell inserts) and decreased impedance measurements (from 60–72 h), the real-time horizontal impedance measurements started 2 d postseeding to prevent effects of dome formation on these measurements. DON was added at increasing concentrations (0, 1.39, 4.17, and 12.5 µM) applied in temperature-equilibrated medium, followed immediately by real-time impedance measurements every 5 min over a period of 24 h. Impedance measurements were recorded at frequencies of 10, 25, and 50 kHz, from which a compound signal, referred to as the cell index, was created (25). The relative change in impedance at a certain time point was calculated by dividing the cell index value by the reference time point (time 0) and corrected in relation to the control condition. Area under the curve (AUC) of each replicate was calculated for statistical analysis.

In vitro *expression of TJ proteins: isolation of RNA and qRT-PCR analysis of Caco-2 cells*

Caco-2 cell monolayers were grown on inserts and exposed to increasing concentrations of DON in the apical and basolat-

eral compartments for 3, 6, and 24 h. Thereafter, cells were washed twice with ice-cold PBS and were harvested into 100 μl RNA lysis buffer with β-mercaptoethanol. Total RNA was isolated using spin columns (Promega) according to the manufacturer's instructions. RNA amounts were determined spectrophotometrically, and RNA purity was measured by NanoDrop 2000 (Thermo Scientific, Waltham, MA, USA) as A_{260}/A_{280} ratio with expected values between 1.8 and 2. Subsequently, 1 μg of extracted total RNA was reverse transcribed with the iScriptTM cDNA Synthesis kit (Bio-Rad Laboratories, Hercules, CA, USA). The cycling protocol for 20 μl reaction mixes was 5 min at 25°C, followed by 30 min at 42°C, and 5 min at 85°C to terminate the reaction. After reverse transcription, cDNA was stored at −20°C. cDNA was diluted with nuclease-free water (1:9) directly before qRT-PCR analysis. The reaction mixture for the qRT-PCR, containing 10 μl of the diluted cDNA mixed with 12.5 μl iQSYBR Green Supermix (Bio-Rad Laboratories), forward and reverse primers (final concentration of 300 nM for each primer), and sterile deionized water, was prepared according to manufacturer's instructions. qRT-PCR was performed using the MyIQ single-color real-time PCR detection system (Bio-Rad Laboratories) and MyIQ System 1.0.410 software (Bio-Rad Laboratories). PCR cycle parameters were as follows: general denaturation at 95°C for 3 min, 1 cycle, followed by 40 cycles of 95°C for 20 s, annealing temperature (AT) for 30 s, and elongation at 72°C for 30 s. Gene-specific primers for CLDN1, CLDN 3, CLDN4, OCLN, and ZO protein 1 (ZO-1) (**Table 1**) were derived from the U.S, National Center for Biotechnology Information (NCBI; Bethesda, MD, USA) GenBank and were manufactured commercially (Eurogentec, Seraing, Belgium). Specificity and efficiency of selected primers (Table 1) were confirmed by qRT-PCR analysis of dilution series of pooled cDNA at a temperature gradient (55–65°C) for primer annealing and subsequent melting curve analysis. The geNorm 3.5 software (Ghent University, Ghent, Belgium) was used to identify the most stable reference genes for this experiment. The mRNA quantity was calculated relative to the expression of two reference genes, glyceraldehyde 3-phosphate dehydrogenase (GAPDH) and β-actin (ACTB). No significant effect of DON exposure on the C_t values of GAPDH and ACTB compared to the unstimulated cells (0 μM DON) was observed (data not shown).

Western blot analysis

Caco-2 cell monolayers were grown on inserts and incubated with increasing concentrations of DON in the apical and basolateral compartments for 24 h. Caco-2 monolayers were washed twice with cold PBS, and cells were lysed with 50 μl RIPA lysis buffer (50 mM Tris, 150 mM NaCl, 0.5% DOC, 1% Nonidet P-40, and 0.1% SDS, pH 8.0; Thermo Scientific) containing protease inhibitors (Roche Applied Science). After 5 min incubation with RIPA buffer, monolayers were harvested and centrifuged at 14,000 g for 15 min to yield a clear lysate. Total protein content was determined using the BCA protein assay (Thermo Scientific) following the manufacturer's instructions. Equal protein amounts of heat-denaturated nonreduced samples were separated electrophoretically (Criterion gel, 4–20% Tris-HCL; Bio-Rad Laboratories) and electrotransferred onto polyvinylidene difluoride membranes (Bio-Rad, Veenendaal, The Netherlands). The membranes were blocked with PBS containing 0.05% Tween-20 (PBST) and 5% milk proteins for 1 h at room temperature. Subsequently, the primary antibodies CLDN1, CLDN3, CLDN4, OCLN, and ZO-1 (Invitrogen; see Supplemental Table S1), diluted according to manufacturer's instructions, were incubated overnight at 4°C, followed by washing the blots in PBST. Secondary antibodies (Dako, Glostrup, Denmark) were applied for 2 h at room temperature. Blots were washed in PBST and incubated in commercial ECL reagents (Amersham Biosciences, Roosendaal, The Netherlands), and exposed to photographic film. Membranes were subsequently reprobed with rabbit monoclonal anti-human ACTB antibody (Cell Signaling, Danvers, MA, USA; see detailed information in Supplemental Table S1) to assess homogeneity of loading. Films were scanned on a GS710 calibrated imagine densitometer (Bio-Rad Laboratories) and the optical density (OD) for the immunoreactive bands was quantified.

Immunofluorescence staining Caco-2 cells

Cellular localization of TJ proteins was assessed by immunofluorescence. Caco-2 cells were grown on inserts and exposed to 4.17 μM DON in the apical and basolateral compartments for 24 h. Subsequently, the inserts with cells were fixed with 10% formalin for 10 min. After washing with PBS, the cells were permeabilized with PBS containing 0.1% Triton-X-100 for 5 min, and blocked with 5% serum for 30 min at room temperature. Thereafter, the samples were incubated (2 h, room temperature) with different primary antibodies CLDN1, CLDN3, CLDN4, OCLN, and ZO-1 (Invitrogen; see Supplemental Table S1) diluted in PBS containing 1% BSA according to manufacturer's instructions. The negative control lacking the primary antibodies was included (Supplemental Fig. S3). Samples were rinsed with PBS followed by incubation with Alexa-Fluor conjugated secondary antibody (Life Technologies) for 1 h at room temperature. A nuclear counterstaining was performed by incubating the samples for 1–3 min with Hoechst 33342 (1:2000; Invitrogen). After washing, the inserts were mounted with ProLong Gold antifade reagent. Immunolocalization of TJ proteins was visualized and images were taken using the Nikon Eclipse TE2000-U microscope equipped with a Nikon Digital Sight DS-U1 camera.

TABLE 1. *Human primer sequences used for qRT-PCR analysis*

| Target gene | Primer sequence, 5′-3′ | | AT | Reference |
	Forward	Reverse		
CLDN1	AGCTGGCTGAGACACTGAAGA	GAGAGGAAGGCACTGAACCA	63	NM_021101
CLDN3	CTGCTCTGCTGCTCGTGTC	CGTAGTCCTTGCGGTCGTAG	63	NM_001306
CLDN4	GTCTGCCTGCATCTCCTCTGT	CCTCTAAACCCGTCCATCCA	62.5	NM_001305
OCLN	TTGGATAAAGAATTGGATGACT	ACTGCTTGCAATGATTCTTCT	57	NM_002538
ZO-1	GAATGATGGTTGGTATGGTGCG	TCAGAAGTGTGTCTACTGTCCG	55.8	NT_010194.17
GAPDH	ACCCACTCCTCCACCTTTGAC	CCACCACCCTGTTGCTGTAG	62.4	NM_002046
ACTB	CTGGAACGGTGAAGGTGACA	AAGGGACTTCCTGTAACAATGCA	63	NM_001101

AT, annealing temperature (°C).

In vivo experiments

Animals

Male B6C3F$_1$ mice (n=5–6/group), 6–7 wk old (Charles River Laboratories, Maastricht, The Netherlands) were housed under controlled conditions in standard laboratory cages and were acclimated to the in-house environment for 2 wk. The room was maintained on a 12-h light-dark cycle at ~20.5°C with a relative humidity of ~61.5%. The AIN-93G-based diet (26), composed by Research Diet Services (Wijk-bij-Duurstede, the Netherlands), and water were provided *ad libitum*. The AIN-93G-based diet was checked for DON contamination by standard HPLC analyses with affinity column cleanup based on the method described in Dombrink-Kurtzman *et al.* (27), and no DON contamination exceeding the limit of 10 μg/kg feed was detected. All *in vivo* experimental protocols were approved by the Ethics Committee for Animal Experiments (DEC 2012.III.02.012) and were performed in compliance with governmental and international guidelines on animal experimentation.

DON gavage and FITC-dextran permeability assay

Feed was withdrawn from cages 2 h before toxin administration. DON, dissolved in 200 μl PBS, was administered at a dose of 25 mg/kg BW by oral gavage. Control animals received 200 μl of vehicle. The 25 mg/kg dose represents approximately one-third to one-half of the LD$_{50}$ for DON in mice (28). At 2 h after DON administration, all animals received FITC-dextran (500 mg/kg BW; molecular mass 4 kDa; Sigma-Aldrich) by an oral gavage. The appearance of FITC-dextran in blood serum was measured 4 h after the FITC-dextran gavage (6 h after DON administration). Directly after cervical dislocation, blood was obtained by heart puncture and collected in MiniCollect Z Serum Sep tubes (Greiner Bio-One). After 1 h, the clotted blood samples were centrifuged for 10 min at 14,000 rpm and the sera were collected. Standard curves were obtained by a serial dilution of FITC–dextran in serum of mice that did not receive FITC-dextran and were not included in this experiment.

Serum samples from treated animals were diluted in an equal volume of PBS and the amount of FITC-dextran determined by measuring the fluorescence intensity using a spectrofluorometer (FLUOstar Optima; BMG Labtech) set at excitation and emission wavelengths of 485 and 520 nm, respectively.

In vivo expression of TJ proteins: isolation of RNA and qRT-PCR of mouse intestinal samples

For mRNA studies, the mouse intestine was flushed with cold PBS and separated into different segments. These segments were defined as follows: proximal small intestine (first centimeter of the proximal part of the jejunum, ~2 cm after the stomach), middle small intestine (part of the intestine 7–8 cm after the first centimeter of the proximal part of the jejunum), distal small intestine (final centimeter before the ileum-caecum-colon junction), caecum, and colon. These whole intestinal wall samples (~1 cm) were snap-frozen in liquid nitrogen and stored at −80°C for RNA isolation. Next, 50 mg of each sample was suspended into 350 μl RNA lysis buffer with β-mercaptoethanol and homogenized using a TissueLyser (Qiagen, Hilden, Germany) for 1 min at 25 Hz. RNA isolation, cDNA synthesis, and qPCR reactions were performed as described for the *in vitro* experiments. Primer sequences with corresponding annealing temperatures are listed in **Table 2**.

Immunofluorescence staining of mouse intestinal specimens

The distal small intestine and colon (4–5 mice/group) were fixed in 10% neutral buffered formalin and embedded in paraffin as a "Swiss roll" (29) to permit a complete microscopic examination. After paraffin embedding, 5-μm sections were cut (2–3 sections/antibody/animal). These Swiss-rolled paraffin sections were deparaffinized, endogenous peroxidase activity was blocked with 0.3% H$_2$O$_2$ (Merck, Darmstadt, Germany) in methanol for 30 min at room temperature and rehydrated in a graded ethanol series to PBS. For antigen retrieval, the slides were boiled in 10 mM citrate buffer (pH 6.0) for 10 min in a microwave. The slides were cooled down to room temperature, rinsed with PBS (3×) and blocked with 5% serum for 30 min at room temperature. Thereafter, the immunofluorescence staining protocol with the primary antibodies CLDN1, CLDN2, CLDN3, CLDN4, OCLN (Invitrogen), and ZO-1 (Millipore) (see Supplemental Table S1) was performed as described above. The negative controls lacking the primary antibodies were included (Supplemental Fig. S3*B–D*).

Histomorphometric analysis of mouse intestines

The proximal small intestine and distal small intestine were fixed in 10% neutral buffered formalin and embedded as a Swiss roll (29). After paraffin embedding, 5-μm sections were cut and stained with hematoxylin and eosin (H&E) according to standard methods. Photomicrographs were taken with an

TABLE 2. *Murine primer sequences used for qRT-PCR analysis*

| Target gene | Primer sequence, 5′-3′ | | AT | Reference |
	Forward	Reverse		
CLDN1	TCTACGAGGGACTGTGGATG	TCAGATTCAGCTAGGAGTCG	57	NM_016674
CLDN2	GGCTGTTAGGCTCATCCAT	TGGCACCAACATAGGAACTC	55	NM_016675
CLDN3	AAGCCGAATGGACAAAGAA	CTGGCAAGTAGCTGCAGTG	58.7	NM_009902
CLDN4	CGCTACTCTTGCCATTACG	ACTCAGCACACCATGACTTG	55	NM_009903
OCLN	ATGTCCGGCCGATGCTCTC	TTTGGCTGCTCTTGGGTCTGTAT	61.2	NM_008756.2
ZO-1	CGAGGCATCATCCCAAATAAGAAC	TCCAGAAGTCTGCCCGATCAC	58.7	NM_009386
GAPDH	GAACATCATCCCTGCATCC	CACATTGGGGGTAGGAACAC	61	NM_008084.2
ACTB	ATGCTCCCCGGGCTGTAT	CATAGGAGTCCTTCTGACCCATTC	61	NM_007393.3

AT, annealing temperature (°C).

Olympus BX50 microscope (Olympus Europa GmbH, Hamburg, Germany) equipped with a Leica DFC 320 digital camera (Leica Microsystems, Wetzlar, Germany). The morphometric analysis of the sections was performed on 10 randomly selected, well-oriented villi and crypts per animal. A computerized microscope-based image analyzer (Cell^D; Olympus) was used to determine histomorphometric parameters: villus height (measured from the tip of the villus to the villus-crypt junction), crypt depth (measured from the crypt-villus junction to the base of the crypt), villus width, villus surface area (total surface of the villus) and epithelial cell area (villus area minus villus area without epithelial cells). These regions of interest were manually defined for each villus separately; an example of the histomorphometric analysis of a villus is depicted in Supplemental Fig. S1.

Statistical analyses

Experimental results are expressed as means ± SEM. Analyses were performed by using GraphPad Prism 5.0 (GraphPad, La Jolla, CA, USA). Differences between groups were statistically determined by using 1-way ANOVA, with Bonferroni *post hoc* test for *in vitro* experiments and an unpaired 2-tailed Student's *t* test for *in vivo* experiments. Results were considered statistically significant when $P < 0.05$.

RESULTS

Cytotoxic effects of DON in Caco-2 cells

The direct cytotoxicity of DON was measured over a concentration range between 0 and 37.5 µM by the LDH leakage assay. DON did not impair cell viability, as indicated by LDH release in apical and basolateral compartments up to a concentration of 12.5 µM. LDH release increased slightly, but not significantly, at this concentration (**Fig. 1**). In all forthcoming experiments, DON concentrations ≤12.5 µM were used.
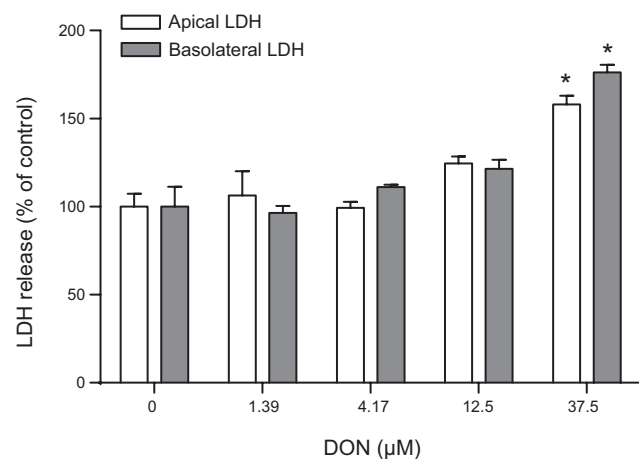

Figure 1. DON did not exert cytotoxic effects on Caco-2 cells. Caco-2 cells grown on inserts were incubated with increasing concentrations of DON (0, 1.39, 4.17, 12.5, and 37.5 µM) for 24 h, followed by measurement of LDH release in the apical as well as the basolateral compartment of the transwell insert system. Results are expressed as mean ± SEM percentage of LDH released by the nontreated cells of 3 independent experiments, each performed in triplicate.

Effects of DON on TEER of a Caco-2 monolayer

On exposure to increasing concentrations of DON (0, 0.05, 0.15, 0.46, 1.39, 4.17, and 12.5 µM) added to the apical and basolateral compartments, a clear dose-response curve was obtained. Concentrations up to 0.46 µM DON remained without any effect, whereas the following test concentration of 1.39 µM resulted in a highly significant decrease of the TEER value (**Fig. 2***A*). To assess the differences in the routes of exposure, DON was added to either the apical or the basolateral side, or to both sides of the transwell chamber (Fig. 2*B*). Results show that after basolateral exposure to DON, the decrease of TEER values was more pronounced compared to the alterations observed after apical exposure to DON (Fig. 2*B*), where only small effects were observed. The TEER decrease after dual exposure to DON from the apical and basolateral side was comparable with the decrease in TEER values after basolateral exposure (Fig. 2*B*). Since, DON is quickly and expeditiously absorbed in the upper parts of the small intestine (30), and following absorption it is likely to be secreted into the gut lumen as DON is a substrate for ABC efflux transporters (31), exposure to both apical and basolateral side mimics the *in vivo* situation and will be used in the following experiments. The time dependency was established in experiments using increasing concentrations of DON (1.39, 4.17, and 12.5 µM), which were added to the apical as well as to the basolateral side. Different incubation time points (2, 4, 8, 12, and 24 h) were tested, and a time-dependent decrease in TEER was observed (Fig. 2*C*). The first significant TEER decrease by DON was observed after 8 h.

DON increases permeability of Caco-2 monolayer

Monitoring the permeability of the paracellular transport markers LY (0.457 kDa) and two different molecular sizes of FITC-dextran (4 and 40 kDa, respectively) across the cell monolayer (**Fig. 3**) indicated that DON (added to both apical and basolateral compartments) induced a significant increase in the translocation of LY (0.457 kDa) and 4 kDa FITC-dextran from the apical to the basolateral chamber (Figs. 3*A* and **4***B*). However, DON exposure (both apical and basolateral) did not affect the Caco-2 monolayer permeability of 40-kDa FITC-dextran, which remained unchanged (Fig. 3*B*).

DON induces a decline in impedance values after real-time monitoring

Real-time recording of the horizontal impedance every 5 min over a period of 24 h following exposure of a Caco-2 monolayer to 3 different concentrations of DON (1.39, 4.17, and 12.5 µM) showed an immediate and concentration-dependent decline in impedance values commencing within the first 15 min of DON exposure and lasting for almost the entire observation period (Fig. 4*A*). Lines of individual experiments were summarized as AUC, and this summary measure was used for statistics (in a separate
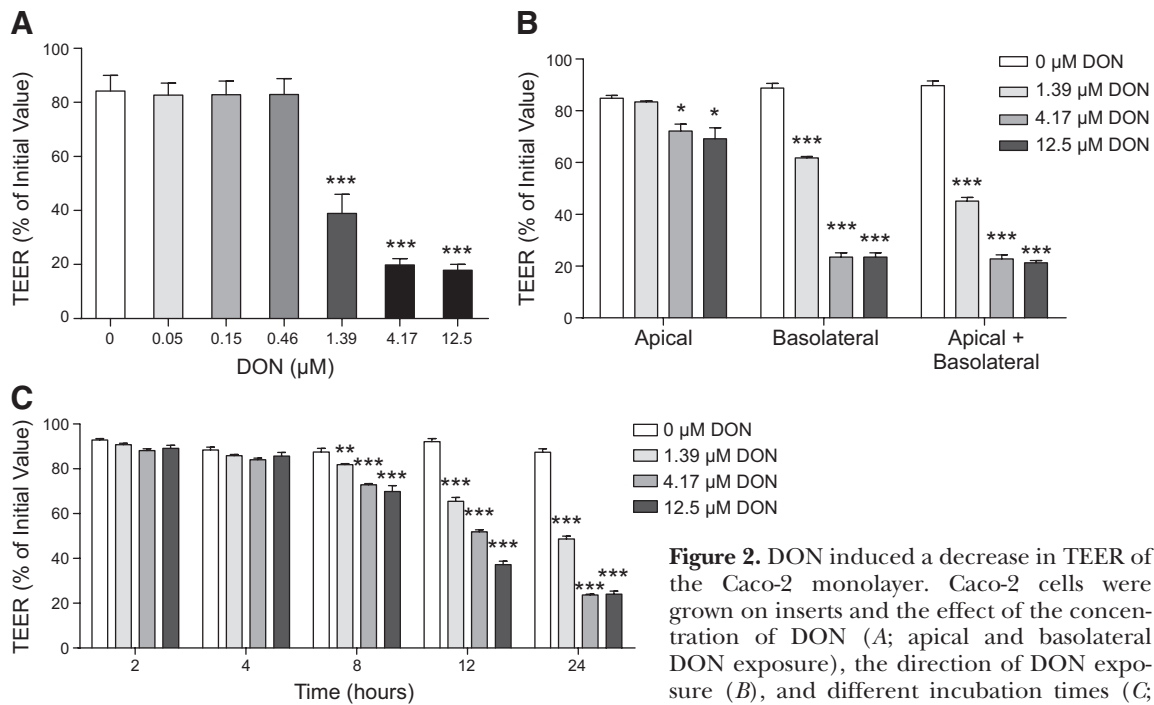
Figure 2. DON induced a decrease in TEER of the Caco-2 monolayer. Caco-2 cells were grown on inserts and the effect of the concentration of DON (*A*; apical and basolateral DON exposure), the direction of DON exposure (*B*), and different incubation times (*C*; apical and basolateral DON exposure) were examined. Subsequently, the TEER was measured as described in Materials and Methods. Results are expressed as mean $\pm$ SEM percentage of initial value of 3 independent experiments, each performed in triplicate. *$P \leq 0.05$, **$P < 0.01$, ***$P < 0.001$ *vs.* 0 µM DON.

panel, Fig. 4*B*). *P* values are from 1-way ANOVA tests to statistically determine the differences between groups.

DON up-regulates mRNA expression of TJ proteins in Caco-2 cells

To correlate the DON-induced impaired integrity with barrier dysfunctions, the mRNA expression levels of the different TJ proteins (CLDN1, CLDN3, CLDN4, OCLN, and ZO-1) were measured. Caco-2 cell monolayers, grown on inserts, were exposed to increasing concentrations of DON (1.39, 4.17, and 12.5 µM) in the apical and basolateral compartments for 3, 6, or 24 h. RT-PCR analysis demonstrated that already after 3 h of DON exposure, the mRNA expression levels of CLDN3, CLDN4, and ZO-1 were up-regulated in a concentration-dependent manner (**Fig. 5*A***). After 6 h of DON exposure, the mRNA expression levels of all TJ proteins were dose-dependently increased (Fig. 5*B*). The mRNA expression of the TJ proteins in Caco-2 cells after 24 h of DON
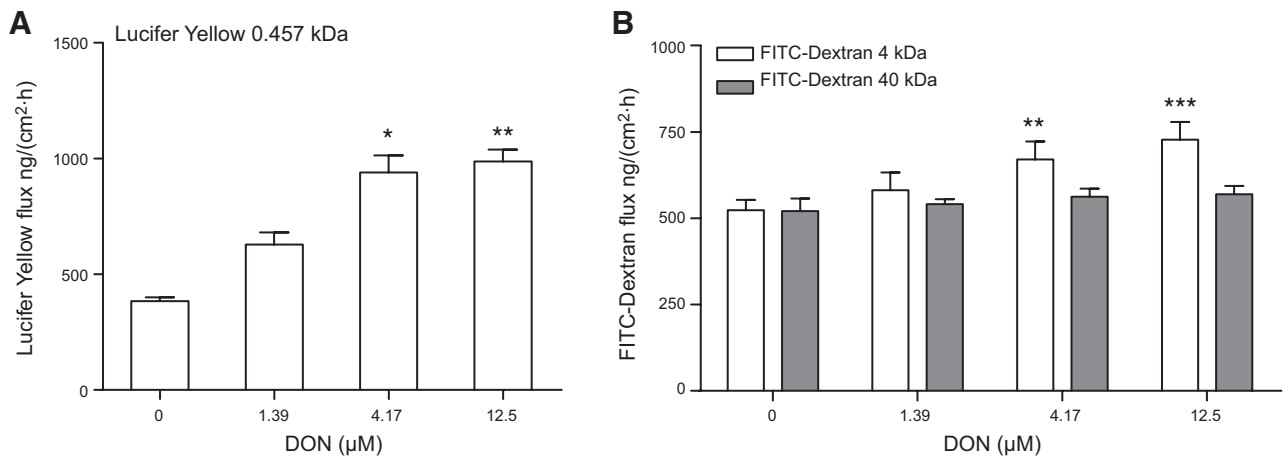

Figure 3. DON increased the permeability of the Caco-2 monolayer. Caco-2 cells were grown on inserts and stimulated with increasing concentrations of DON in the apical and basolateral compartments for 24 h. Subsequently, the translocation of LY (0.457 kDa; *A*) and 2 molecular sizes of FITC-dextran (4 and 40 kDa; *B*) from the apical to the basolateral chamber was performed, as described in Materials and Methods. Results are expressed as mean $\pm$ SEM marker transport (ng·cm^{-2}·h^{-1}) of 3 independent experiments, each performed in triplicate. *$P \leq 0.05$, **$P < 0.01$, ***$P < 0.001$ *vs.* 0 µM DON.
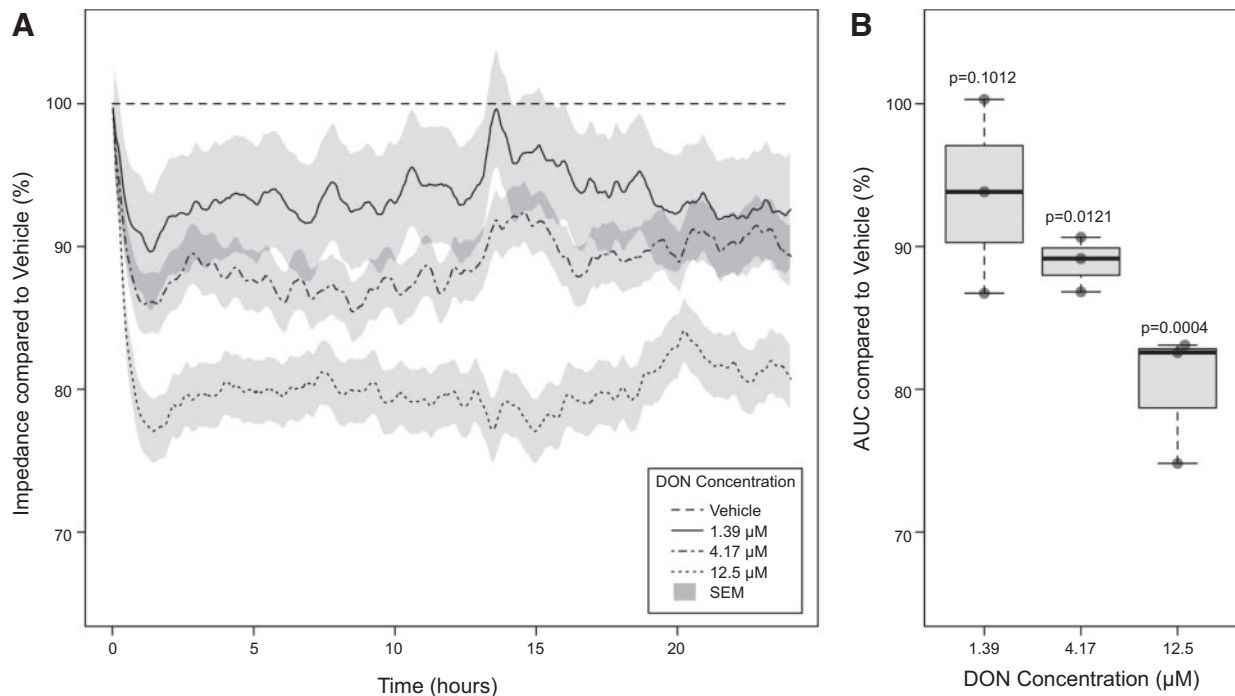
Figure 4. Real-time monitoring of DON-induced epithelial barrier dysfunction. *A*) Caco-2 cells were grown on E-plates to form a monolayer and were incubated with increasing concentrations of DON (0, 1.39, 4.17, and 12.5 μM) for 24 h. Real-time resistance was monitored every 5 min, as described in Materials and Methods. Results are expressed as mean ± SEM relative change in impedance (%) of 3 independent experiments, each performed in quadruplicate. *B*) AUC of each replicate was calculated for statistical analysis. Results are expressed as mean ± SEM percentage AUC *vs.* vehicle (0 μM DON) of 3 independent experiments, each performed in quadruplicate.

exposure was comparable with the results after 6 h of DON exposure (Fig. 5*C*).

DON selectively affects TJ protein levels in Caco-2 cells

Next to the assessment of mRNA expression of the TJ proteins, the effect of DON on the protein levels of several TJs (CLDN1, CLDN3, CLDN4, OCLN, and ZO-1) were quantified by Western blot analysis in Caco-2 cell lysates of cells that had been exposed to DON in the apical and basolateral compartments for 24 h. A representative blot of each TJ protein and the corresponding ACTB used as loading control are shown in **Fig. 6*A, B*** (additional blots are available in Supplemental Fig. S2). The optical density of the molecular weight bands of the different TJ proteins was measured and after normalization with ACTB also depicted in Fig. 6*A, B*. A dose-dependent reduction of the CLDN1, CLDN3, and CLDN4 protein levels was observed in DON-exposed Caco-2 cells compared to untreated cells (Fig. 6*A*). The OCLN and ZO-1 levels remained unchanged after DON challenge (Fig. 6*B*).

DON affects distribution pattern of TJ proteins in Caco-2 cells

To investigate the cellular localization of TJ proteins, Caco-2 cell monolayers grown on inserts were incubated with or without DON (4.17 μM) at apical and basolateral compartments for 24 h, followed by an immunofluorescent staining. In the intact Caco-2 cells, CLDN1, CLDN3,

CLDN4, OCLN, and ZO-1 are localized at the cell membrane and appeared as continuous belt-like structures encircling the cells at the contact points with adjacent cells (Fig. 6*A, B*). DON exposure disturbed the continuity of all tested TJ proteins, which appeared to be irregular distributed in the cells (Fig. 6*A, B*).

In vivo exposure of B6C3F1 mice to DON results in increased intestinal permeability

To confirm the DON-induced hyperpermeability observed in the Caco-2 monolayer, an *in vivo* intestinal permeability assay was performed in a mouse model using the paracellular tracer FITC-dextran (4 kDa). This tracer was significantly increased in serum of DON-treated mice when measured 4 h after a FITC-dextran oral gavage (**Fig. 7**). This finding indicates that DON induced an increase in the *in vivo* intestinal permeability observed by the translocation of FITC-dextran across the intestinal interfaces in B6C3F$_1$ mice.

DON selectively up-regulates mRNA expression of TJ proteins in different parts of mouse intestines

To extrapolate the DON-induced induction in mRNA expression of different TJ proteins observed in Caco-2 cells, the mRNA expression levels of the same TJ proteins (CLDN1, CLDN2, CLDN3, CLDN4, OCLN, and ZO-1) were measured in different segments of the mouse intestines (proximal, middle, and distal small intestine, caecum, and colon). CLDN4 mRNA expres-
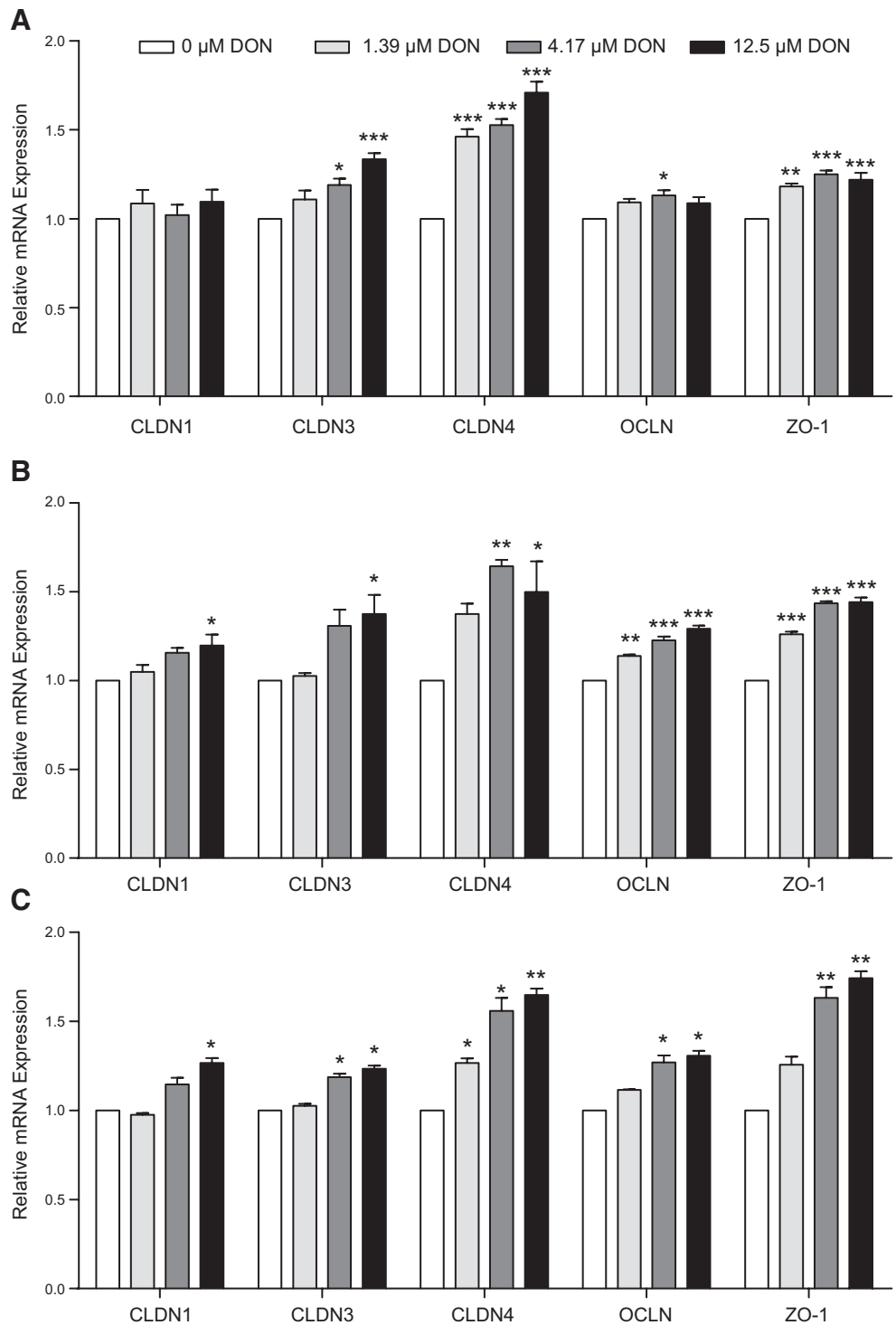
Figure 5. DON up-regulated mRNA expression of TJ proteins in Caco-2 cells. Caco-2 cells were grown on inserts and stimulated with increasing concentrations of DON (1.39, 4.17, and 12.5 μM) in apical and basolateral compartments for 3 (*A*), 6 (*B*), and 24 h (*C*). mRNA levels of TJ proteins (CLDN1, CLDN3, CLDN4, OCLN, and ZO-1) were measured by qRT- PCR, as described in Materials and Methods. Results are expressed as mean ± sem relative mRNA expression of 3 independent experiments, each performed in triplicate. *$P \le 0.05$, **$P < 0.01$, ***$P < 0.001$ *vs.* 0 μM DON.

sion levels were increased in all parts of the intestines of the DON-treated animals compared to the control animals (**Fig. 8*A–E***), whereas CLDN3 expression levels were increased after DON gavage in all parts of the intestines, except the proximal and middle small intestine (Fig. 8*C–E*). The mRNA expression levels of CLDN2 were increased in the mouse middle and distal small intestine on DON exposure as compared to the nontreated animals (Fig. 8*B, C*).

The ZO-1 mRNA expression levels were only increased in the proximal small intestine of the DON-treated ani-

mals (Fig. 8*A*). The mRNA expression of OCLN and CLDN1 remained unaffected in all parts of the intestines of DON-exposed mice compared to control mice.

DON affects distribution pattern of TJ proteins in intestines of mice

Considering that DON selectively up-regulated the mRNA levels of the TJ proteins in the mouse intestines, especially in the distal part of the small intestine, immunofluorescence stainings of all TJ proteins

(CLDN1, CLDN2, CLDN3, CLDN4, OCLN, and ZO-1) were performed to show the cellular distribution and localization of TJ proteins. Results show that in the distal small intestine of control mice, CLDN1 and CLDN3 were expressed laterally between adjacent cells with neither a specific signal at the apical cell surface nor on the basal membrane. After DON gavage, the CLDN1 and CLDN3 expression was more pronounced laterally and at the basal cytoplasm (Fig. 8F). CLDN2 distribution was restricted to the villus crypts in the distal small intestine of control animals and was expressed laterally between adjacent cells. This CLDN2 expression pattern was disrupted after DON gavage. In contrast to the controls, CLDN2 expression was not restricted to the villus crypts anymore (Fig. 8F). CLDN4 was expressed in both the tips and crypts of the villi in the distal small intestine. These findings clearly indicate that the expression of CLDN4 is restricted to selective sites and cannot be found on every tip or crypt of the villus epithelium. No pronounced effect on the CLDN4 distribution pattern in the distal small intestine was observed after the DON gavage (Fig. 8F). Unlike the distribution pattern of the CLDNs, expressed laterally between adjacent cells in the distal small intestine, OCLN and ZO-1 were localized in distinct dot-like structures at the apical region of the lateral plasma membrane of the epithelial cells of a villus, and no clear alterations were observed after DON exposure (Fig. 8F). In addition, immunofluorescence stainings of different TJ proteins (CLDN1, CLDN2, CLDN3, CLDN4, OCLN, and ZO-1) were performed in the colon of control and DON-treated animals, to investigate whether the distribution pattern of TJ proteins in the colon is affected by DON. No clear differences in the TJ distribution patterns of CLDN1, CLDN2, CLDN3, CLDN4, OCLN, and ZO-1 were observed in the colon of DON-treated animals compared to control animals (Supplemental Fig. S4).

DON induces histomorphological changes in intestines of mice

A quantitative histomorphometric analysis of the proximal and distal small intestine showed a significant decrease in villus height and villus area in the proximal (**Fig. 9A**) as well as in the distal small intestine (Fig. 9B) of DON-exposed mice in comparison to the nontreated animals. Furthermore, the epithelial cell area of the DON-treated mice was also significantly diminished in both proximal (Fig. 9A) and distal small intestine (Fig. 9B). The crypt depth was only increased in the proximal small intestine of the DON-treated mice compared to nontreated mice (crypt depth: control, 131.71 ± 5.20 μm; DON, 168.50 ± 7.65 μm; $P \leq 0.01$), while no changes in villus width were observed in both parts of the small intestine followed by DON treatment.

DISCUSSION

A compromised intestinal barrier function has been associated with various diseases, including inflammatory bowel disease, celiac disease, and irritable bowel syndrome. It is generally assumed that the primary cause leading to such a loss of intestinal integrity remains often unknown and is believed to be multifactorial. In this study, we hypothesized that one of the factors that compromises the intestinal barrier function is the fungal toxin DON. DON is a secondary metabolite and exotoxin of various fungal species of the genus *Fusarium*, which are soil-borne and invade living plants prior to harvest. As a small molecule (molecular weight 296.3), it resists technical processes of milling and food processing and can be detected in various food commodities. The high incidence of human exposure is confirmed by the analysis of urine samples for DON and its glucuronides, demonstrating that the exposure incidence exceeds, in many cases, 90% of the tested population (18–21). Experimental data showed that DON inhibits cellular protein synthesis and exerts a ribosomal stress syndrome associated with an inflammatory response, as recently reviewed by Pestka (32) and He *et al.* (33). Initially, incidental and human exposure to high concentrations of DON was associated with acute gastritis and intestinal distress (15). Recent experimental data with different *in vitro* systems, however, show that DON already at lower dietary concentrations is able to impair the integrity of epithelial cell monolayers. A dysfunctional epithelial cell barrier may be one of the predisposing factors leading to inflammatory diseases such as food allergy, inflammatory bowel disease, and celiac disease. Here we describe a series of experiments designed to identify the cascade of events exerted by DON that lead to the loss of epithelial barrier integrity *in vitro* and a compromised intestinal barrier function *in vivo* in mice exposed orally to DON, resembling human dietary exposure.

Impairment of transepithelial resistance depends on route of exposure

A common early marker of an impairment of epithelial barrier integrity is a decrease in the TEER of an established Caco-2 cell monolayer at DON concentrations that do not affect cell viability. In an initial series of experiments, we demonstrated that concentrations ≤ 12.5 μM DON did not impair Caco-2 cell viability (Fig. 1), a finding that was in agreement with previous results (31). Considering the kinetics of DON, which is rapidly absorbed in the upper intestine (30), but is also secreted into the intestinal lumen, as it is a substrate for ABC efflux transporters (31), we conducted TEER measurements following different routes of exposure. First, increasing concentrations of DON were added to the apical side, mimicking the direct contact of the epithelial cells with contaminated food components. A dose-dependent decrease in TEER of the Caco-2 monolayer was observed after 24 h of DON incubation. This is in agreement with previous studies (12, 13) and the data of De Walle *et al.* (11), who found a dose-dependent decrease in TEER of Caco-2 cells at concentrations between 0.17 and 17 μM of DON after apical exposure of a cell monolayer. In turn, DON was added to the basolateral compartment to
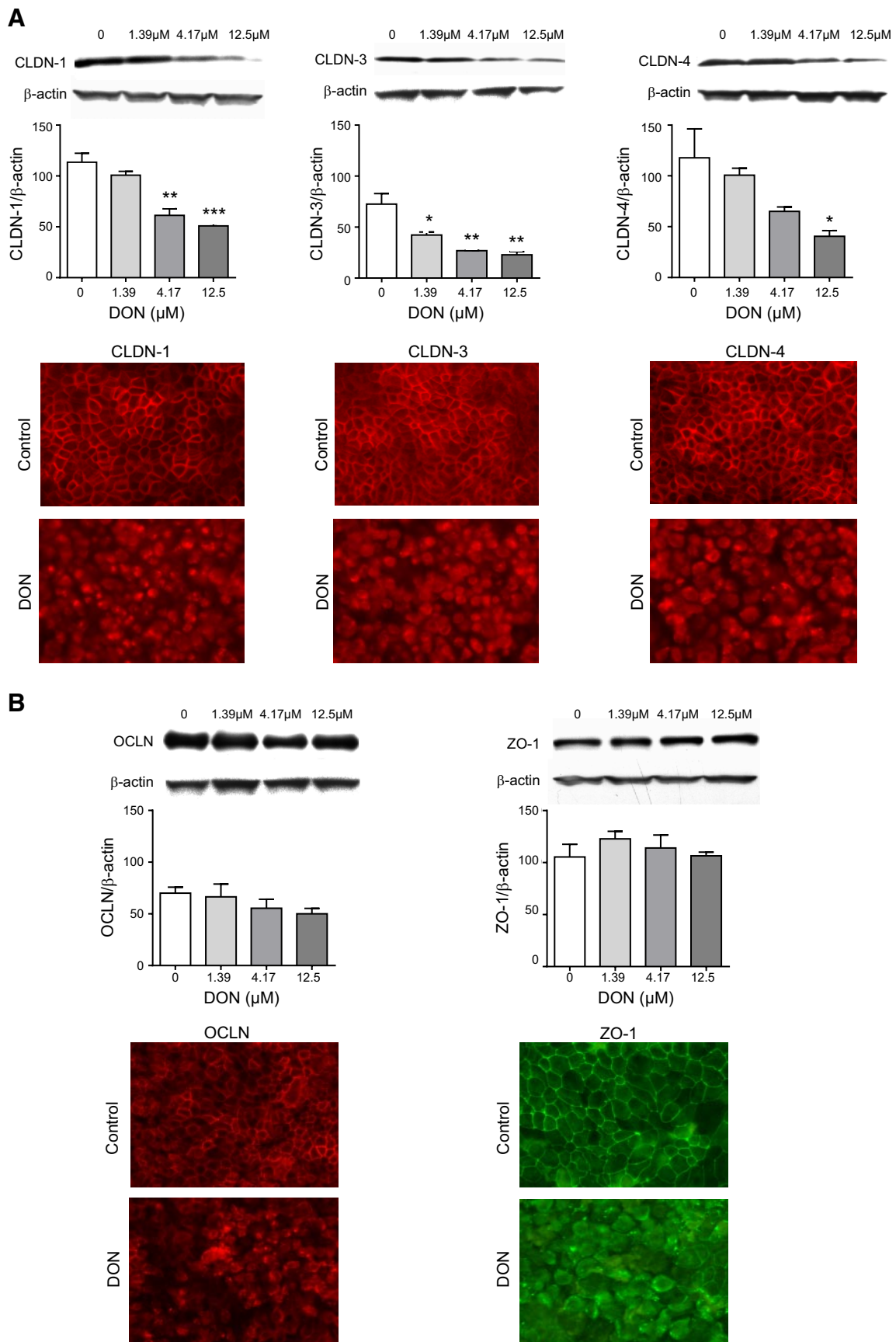
Figure 6. DON selectively affected TJ protein levels and localization. Caco-2 cells were grown on inserts and stimulated with increasing concentrations of DON (1.39, 4.17, and 12.5 μM) in apical and basolateral compartments for 24 h. Caco-2
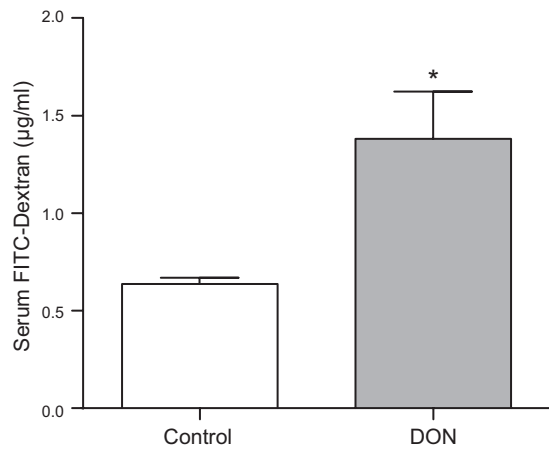
Figure 7. DON increased *in vivo* intestinal permeability in B6C3F$_1$ mice. At 2 h after oral DON administration (25 mg DON/kg BW), mice were gavaged with 4-kDa FITC-dextran (500 mg/kg BW). At 4 h after FITC-dextran gavage, the appearance of FITC-dextran was measured in blood, as described in Materials and Methods Values are expressed as means ± SEM; n = 5–6 animals/group. *$P \leq 0.05$ *vs.* control group.

mimic the secretory pathway of absorbed DON, which is mediated by the efflux transporters ABCB1 (Pg-p) and ABCC2 (MRP2) (31). Interestingly, the decrease in TEER values following basolateral exposure was more pronounced. This finding is in agreement with recent data by Diesing *et al.* (12), reporting that the basolateral surface of the intestinal barrier seems to be more susceptible to DON, as compared to the apical exposure route, in porcine IPEC-J2 cells. To further substantiate these findings, DON was added to both compartments of the transwell system. The measured decrease of TEER values was almost similar to the effects of a basolateral exposure to DON. Besides this dose-dependent effect of DON on the TEER of Caco-2 monolayers after 24 h, a time-dependent decrease in TEER was observed when comparing different incubation time points (2, 4, 8, and 12 h). Although the gastrointestinal transit time of DON ingested with feed is expected to be <1 d, a 24-h DON incubation time is relevant for the *in vivo* situation, since DON is a daily food contaminant of wheat and grain products, and intestinal epithelial cells are regularly exposed to DON during a day. Moreover, Azcona-Olivera *et al.* (28) observed that DON was still measurable in the mouse small (2.50 pmol/mg) and large intestine (7.80 pmol/mg) tissue 24 h after a DON gavage (25 mg/kg). In addition, following absorption in proximal intestine after oral ingestion, DON is likely to be secreted into the colon lumen due to the high expression of efflux transporters along the colon (31).

Impairment of epithelial integrity facilitates a paracellular transport of macromolecules *in vitro* and *in vivo*

The functional consequences of the readily measured impairment of the cell monolayer integrity was demonstrated by measuring the translocation of the paracellular transport markers LY (0.457 kDa) and FITC-dextran (4 and 40 kDa). On 24 h of exposure, DON induced a significant increase in the translocation of LY and 4-kDa FITC-dextran from the apical compartment to the basolateral side. These findings are in agreement with the data of Pinton *et al.* (13, 16), who demonstrated that on 48 h of DON exposure, the Caco-2 and IPEC-1 monolayers became more permeable for 4 kDa FITC-dextran (34). In contrast, we found no difference in the permeability of the 40 kDa FITC-dextran, indicating that larger molecules still cannot pass the epithelial barrier. DON-mediated changes in TJs increase paracellular permeability to small molecules, but not transcellular flux of large molecules as this would require disruption of the cellular layer by cell death. The *in vivo* experiments with B6C3F$_1$ mice, orally exposed to DON confirmed the hyperpermeability as a significant increase in the translocation of FITC-dextran (4 kDa) from the gut lumen to blood circulation was observed in the DON-treated animals. Comparable findings were reported as yet only following exposure of animals to lipopolysaccharide (LPS) and even bacterial pathogens (35, 36).

DON alters function and expression of TJ proteins *in vitro* and *in vivo*

The epithelial barrier function relies on TJs eliminating the intercellular space, like ZO proteins that are perimembrane proteins that link the apical membrane proteins (such as OCLN and CLDNs) with cytoskeleton proteins such as actin (37). Disruption of these actin filaments destroys the TJ protein network, thereby decreasing TEER values (38). The first evidence of a direct effect of DON on the TJ network was obtained by the horizontal impedance measurement. The real-time analysis displayed that DON exposure induced an instant drop in impedance already in the first 1–2 h, followed by a marginal recovery, but not a full recovery, within the 24-h test period. These new findings demonstrate pronounced effects already at concentrations as low as 1.39 µM DON, suggesting a direct effect of DON on TJs, sealing the intercellular space. In this study, the measured impedance is based on different frequencies (10, 25, and 50 KHz) merged to one signal;

monolayers were lysed, and protein extract was analyzed by Western blot analysis for CLDN1, CLDN3, and CLDN4 (*A*) or OCLN amd ZO-1 (*B*) and corresponding ACTB (representative blots are shown). Expression of the proteins was estimated by densitometry after normalization with ACTB. Values are expressed as mean ± SEM ratio [TJ (OD/mm^2)/ACTB (OD/mm^2)] of 3 independent experiments. For immunofluorescence, Caco-2 monolayers were incubated with DON (4.17 µM) at apical and basolateral compartments and detected by antibodies for CLDN1, CLDN3, and CLDN4 (*A*) or OCLN and ZO-1 (*B*), as described in Materials and Methods. View: ×400. *$P \leq 0.05$, **$P < 0.01$, ***$P < 0.001$ *vs.* 0 µM DON.
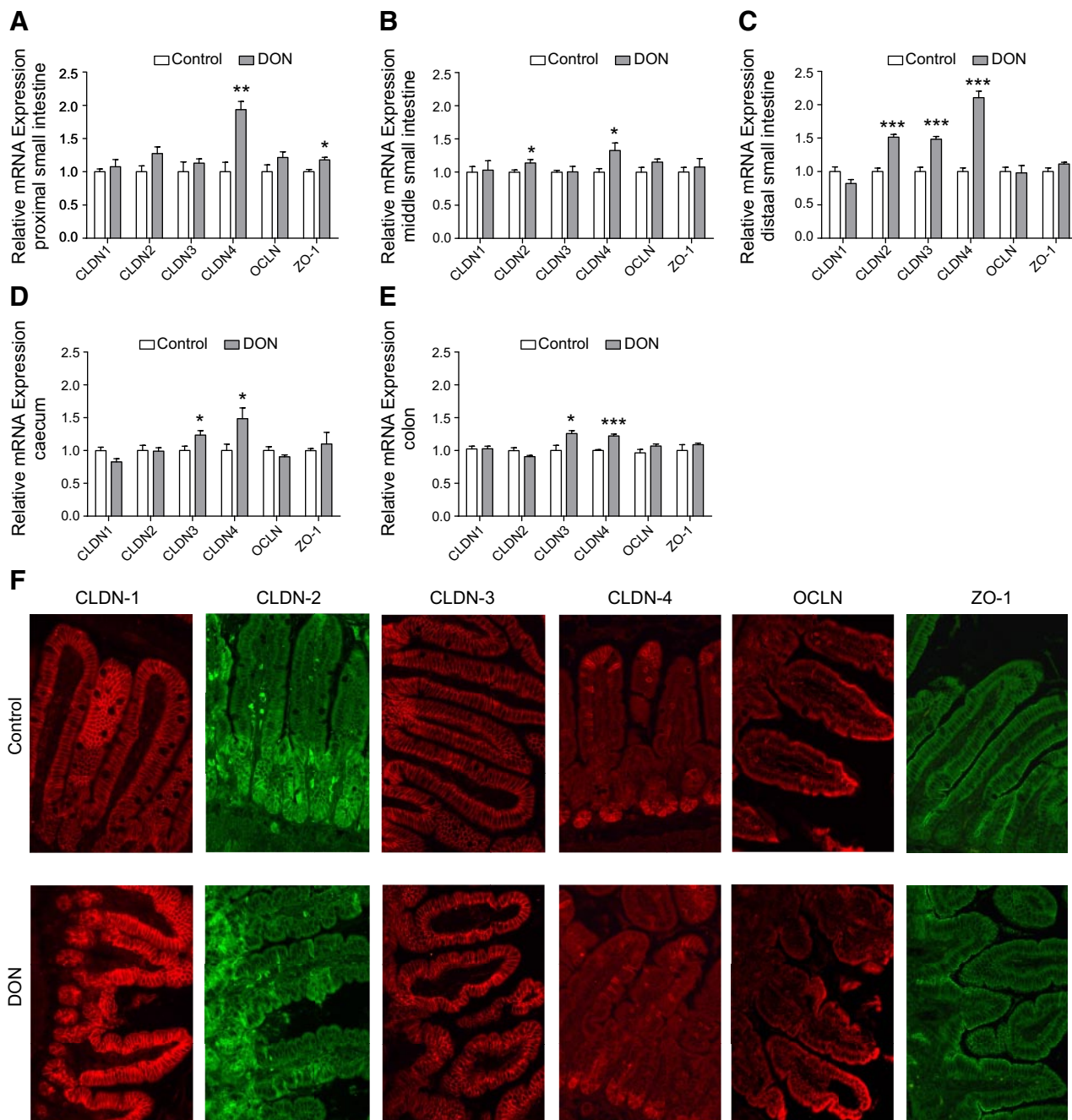
Figure 8. DON selectively affected TJ mRNA expression levels and their localization in mouse intestine. *A–E*) Mice received DON by oral gavage (25 mg DON/kg BW). After 6 h, samples from the proximal small intestine (*A*), middle small intestine (*B*), distal small intestine (*C*), caecum (*D*), and colon (*E*) were collected, and mRNA levels of TJ proteins (CLDN1, CLDN2, CLDN3, CLDN4, OCLN, and ZO-1) were measured by RT-PCR. Results are expressed as mean ± SEM relative mRNA expression; *n* = 5–6 animals/group. *$P \leq 0.05$, **$P < 0.01$, ***$P < 0.001$ *vs.* control group. *F*) For immunofluorescence staining, Swiss-rolled paraffin sections obtained from distal small intestines were detected by antibodies for CLDN1, CLDN2, CLDN3, CLDN4, OCLN, and ZO-1, as described in Materials and Methods. *n* = 4–5 mice/group (2–3 sections/animal). View: ×200.

therefore, we cannot discriminate between transcellular and paracellular impedance contributions. Although, there is a considerable overlap between the real-time impedance and TEER measurements (23), real-time impedance measurements clearly show the time dependency of the events.

Since TEER and impedance measurements suggested alterations of TJ permeability and in order to describe the effect of DON on TJ proteins in more detail, the mRNA expression and protein levels, as well as cellular distribution of different TJ proteins (CLDN1, CLDN3, CLDN4, OCLN, and ZO-1), were measured in Caco-2 cells following DON exposure. PCR analyses pointed out that the mRNA expression of Caco-2 cells exposed to DON for 3 h showed a concentration-dependent up-regulation of the expression levels of CLDN3, CLDN4, and ZO-1, while the mRNA expression levels of all TJ proteins were increased on 6 h of DON exposure,
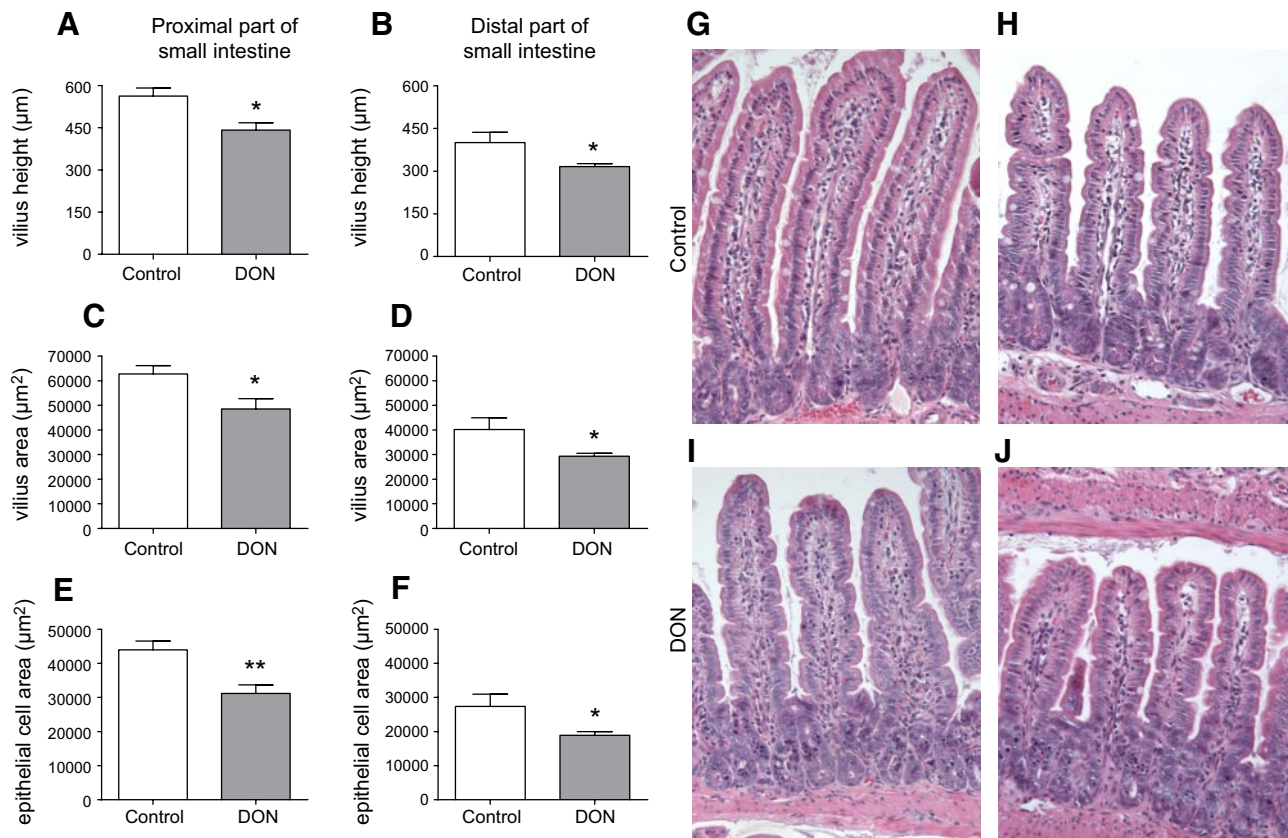
Figure 9. DON induced histomorphological changes in the intestine of mice. Mice received DON by oral gavage (25 mg DON/kg BW); after 6 h, Swiss rolls obtained from the proximal (*A, C, E, G, I*) and distal (*B, D, F, H, J*) small intestine were stained with H&E for histomorphometric analysis of villus height (*A, B*), villus area (*C, D*), epithelial cell area (*E, F*) and related images from control (*G, H*) and DON-treated mice (*I, J*). Magnification 200×. Results are expressed as means ± SEM; *n* = 5–6 animals/group. *P ≤ 0.05, **P < 0.01.

and these results were comparable with the results obtained after 24 h of DON exposure. All individual time points of DON exposure show most probably a compensatory up-regulation of TJ mRNA levels. These results correlate with previous findings with IPEC cells (12) and complete the data of De Walle *et al.* (11) previously showing a raise in the mRNA expression levels of CLDN4 and OCLN in Caco-2 cells exposed to DON for 24 h. These findings were compared again with the *in vivo* mouse model by measuring the mRNA expression levels of TJ proteins after a DON gavage. A direct comparison between the *in vitro* findings in human Caco-2 cells with findings in mice needs to consider possible species differences and the fact that the samples taken in the *in vivo* study contained the entire intestinal wall, not only the epithelial cell layer; however, a number of interesting similarities in the response to DON were observed. For example, in line with the increase in mRNA expression of TJ proteins in DON-stimulated Caco-2 cells, in DON treated mice, the mRNA expression levels of CLDN2, CLDN3, and CLDN4 were significantly increased in different parts of the intestines (small intestine, caecum, and colon), whereas the ZO-1 mRNA expression levels were only increased in the proximal small intestine of the DON-treated animals. The CLDN1 and OCLN mRNA expression was not significantly affected in the treated

mice as compared to the control animals. In the *in vivo* experiments, CLDN2 was measured in addition to CLDN1, CLDN3, and CLDN4, whereas in Caco-2 cells, CLDN2 is normally not expressed (39). The observed up-regulation of the different CLDNs was most pronounced in the distal part of small intestine. The epithelial cells along the distal part of the small intestine are the most susceptible interface in the intestine, most probably because the distal small intestine is exposed to DON from both luminal and basolateral side (40). DON is quickly and expeditiously absorbed in the upper parts of the small intestine (30, 41) and following absorption, it is likely secreted into the gut lumen, as DON is a substrate for the efflux transporters ABCB1 (Pg-p) and ABCC2 (MRP2) (31).

When investigating the protein levels of the TJ proteins CLDN1, CLDN3, CLDN4, OCLN, and ZO-1 in the Caco-2 cells of the *in vitro* DON model, a dose-dependent reduction of the CLDN1, CLDN3, and CLDN4 protein levels in DON-treated Caco-2 cells compared to untreated cells was demonstrated, while the OCLN and ZO-1 levels remained unchanged after DON stimulation. De Walle *et al.* (11) and Pinton *et al.* (13) also showed the absence of a decrease in ZO-1 expression in Caco-2 cells exposed to DON. While these findings reflect the results of the impedance measurements, they also indicate that the TJ network had not entirely

lost its functions. This was also indicated by the observations that very large molecules, such as 40-kDa FITC-dextran, still could not pass the epithelial Caco-2 cell monolayer. These findings are also in agreement with results in other cell lines (11, 12, 16). The decrease in CLDN protein levels is associated with an increase in mRNA expression levels observed after 24 h of DON exposure, which is most likely indicative of a repair mechanism. Whether such repair mechanisms are directly affected by DON at the transcriptional level or are impaired by the previously described nonspecific inhibition of the cellular protein synthesis, as discussed by de Walle *et al.* (11), remains to be elucidated. The effects of the decrease in protein levels and the compensatory up-regulation of mRNA levels of the measured TJ proteins are visualized by the analysis of the cellular localization of TJ proteins in Caco-2 cells. For the immunofluorescence staining, the Caco-2 cells treated with 4.17 µM DON were used, since concentrations from ~0.5 to 7 µM DON represent plausible intestinal DON concentrations that may be found in the gastrointestinal tract after ingestion of moderately to highly DON-contaminated food, as described by Sergent *et al.* (14). The samples of immunofluorescence analysis of Caco-2 cell monolayers show the membrane-associated localization of all TJs, while DON-exposed cells exhibit irregular structures of the stained proteins, suggesting clumping and internalization of fragmented networks. These altered distribution patterns were not only observed for the CLDN proteins, which were dose-dependently decreased, but also for OCLN and ZO-1, for which only marginal alteration in the total immunoreactive protein levels could be measured.

It is becoming increasingly apparent that a variety of pathological stimuli, such as proinflammatory cytokines, microorganisms, and toxins, can induce endocytosis of several TJ proteins and as a consequent internalization of TJs. The internalization of TJs can be accompanied by their advanced degradation or a reallocation to the plasma membrane. However, both mechanisms cause increased paracellular permeability due to the significant loss of TJ proteins at the plasma membrane of epithelial cells (42–46).

Comparable to the *in vitro* and *in vivo* findings, where the most pronounced effects on TJ proteins were observed in the CLDN family, immunofluorescence analysis of the distal small intestine of mice confirmed that DON exposure mainly affected the CLDN distribution.

The lateral distribution pattern of CLDN1 and CLDN3 over the entire villi in the distal small intestine was observed in control mice, and this typical pattern was even more pronounced after DON exposure, resulting additionally in a visible expression at the basal cytoplasm. As already described by Rahner *et al.* (47) and Tamagawa *et al.* (48), CLDN2 is predominantly found in the crypts in mouse small intestine, and this is confirmed in our study, where the CLDN2 was expressed laterally between adjacent cells in the villus crypts. However, after DON gavage this CLDN2 expression pattern is disrupted and not restricted to the crypts anymore, but is distributed along the villi cells. Furthermore, our findings clearly indicate that the expression of CLDN4 is restricted to selective sites, and not found on every tip or crypt of the villus epithelium, which is in agreement with Tamagawa *et al.* (48). No pronounced effect on the CLDN4 distribution pattern in the distal small intestine was observed after the DON gavage. Unlike the distribution pattern of the CLDNs in the distal small intestine, OCLN and ZO-1 were localized in distinct dot-like structures at the apical region of the lateral plasma membrane in the epithelial cells of the villus, and no clear alterations were observed after DON exposure. Immunofluorescence stainings of different TJ proteins were also performed in the colon of control and DON-treated animals to confirm the PCR analyses suggesting that the distal small intestine is most significantly affected by DON. As expected, no clear differences in the TJ distribution patterns of CLDN1, CLDN2, CLDN3, CLDN4, OCLN, and ZO-1 were observed in the colon of DON-treated animals compared to control animals.

Taken together, it can be concluded that the most pronounced effects of DON on TJ proteins involve the CLDN family, as decreased CLDN levels of the DON-treated Caco-2 cells, as well as increased CLDN levels in mouse intestine and an altered CLDN distribution in the distal small intestine on DON stimulation, were observed. Claudins are known to be determinants of functional barrier properties, including size and charge selectivity of the paracellular permeability of the intestinal epithelium (49, 50). It also can be hypothesized that the CLDNs are more susceptible to DON exposure since these transmembrane proteins contain extracellular domains that may act as a binding site for DON as demonstrated for *Clostridium perfringens* enterotoxins interacting with CLDN3 (51). Claudins form a selective barrier between adjacent cells in contrast to the intracellular scaffold protein ZO-1, which interacts with intracellular domains of transmembrane proteins anchoring these proteins to the actin cytoskeleton (52).

A subsequently conducted histomorphometric analysis of the intestinal tissue of the DON-exposed mice showed a significant decrease in villus height, villus area and also in the epithelial cell area in comparison to the nontreated animals. This result is in agreement with the data from Pinton *et al.* (17) reporting a significant reduction in the villus height along jejunum of pigs exposed to a DON-contaminated diet for 4 wk. An *ex vivo* study by Kolf-Clauw *et al.* (53) shows alterations of pig jejunal explants, including shortened and coalescent villi, following DON exposure for 4 h. One possible explanation for the shortened villi could be sloughing of epithelial lining from the surface of the villi and apoptosis and necrosis of the epithelial cells, since the epithelial cell area was also decreased in DON-treated animals. However, no prominent histological lesions were observed. Moreover, after acute mucosal injury by DON (at high dosage), villus contraction can take

place, which is the initial phase of repair mechanisms aiming at the restoration of barrier function by reducing the total and denuded surface area of the villi. Villus contraction can be separated in an immediate contraction and second phase ongoing contraction, which progresses in the first hours after injury and is mediated by endogenous prostaglandins (54).

In summary, the comparison of *in vitro* Caco-2 cell studies with the *in vivo* murine model suggests that the main molecular target of DON in the intestine is the TJ network. Disintegration of this network is accompanied by a loss of barrier function, which increases the risk of antigen transfer and an inflammatory response. Considering the high prevalence of dietary DON exposure in consumers of grains and grain-based products, the possible contribution of DON to the onset and propagation of inflammatory bowel disease warrant further investigation. FJ

REFERENCES

1. Groschwitz, K. R., and Hogan, S. P. (2009) Intestinal barrier function: molecular regulation and disease pathogenesis. *J. Allergy Clin. Immunol.* **124,** 3–20, quiz 21–22
2. Odenwald, M. A., and Turner, J. R. (2013) Intestinal permeability defects: is it time to treat? *Clin. Gastroenterol. Hepatol.* **11,** 1075–1083
3. Menard, S., Cerf-Bensussan, N., and Heyman, M. (2010) Multiple facets of intestinal permeability and epithelial handling of dietary antigens. *Mucosal Immunol.* **3,** 247–259
4. Harhaj, N. S., and Antonetti, D. A. (2004) Regulation of tight junctions and loss of barrier function in pathophysiology. *Int. J. Biochem. Cell Biol.* **36,** 1206–1237
5. Lutz, K. L., and Siahaan, T. J. (1997) Molecular structure of the apical junction complex and its contribution to the paracellular barrier. *J. Pharm. Sci.* **86,** 977–984
6. Balda, M. S., and Matter, K. (2008) Tight junctions at a glance. *J. Cell Sci.* **121,** 3677–3682
7. Schneeberger, E. E., and Lynch, R. D. (1992) Structure, function, and regulation of cellular tight junctions. *Am. J. Physiol.* **262,** L647–L661
8. Hollander, D., Vadheim, C. M., Brettholz, E., Petersen, G. M., Delahunty, T., and Rotter, J. I. (1986) Increased intestinal permeability in patients with Crohn's disease and their relatives. A possible etiologic factor. *Ann. Int. Med.* **105,** 883–885
9. DeMeo, M. T., Mutlu, E. A., Keshavarzian, A., and Tobin, M. C. (2002) Intestinal permeation and gastrointestinal disease. *J. Clin. Gastroenterol.* **34,** 385–396
10. Heyman, M., Abed, J., Lebreton, C., and Cerf-Bensussan, N. (2012) Intestinal permeability in coeliac disease: insight into mechanisms and relevance to pathogenesis. *Gut* **61,** 1355–1364
11. De Walle, J. V., Sergent, T., Piront, N., Toussaint, O., Schneider, Y. J., and Larondelle, Y. (2010) Deoxynivalenol affects in vitro intestinal epithelial cell barrier integrity through inhibition of protein synthesis. *Toxicol. Appl. Pharmacol.* **245,** 291–298
12. Diesing, A. K., Nossol, C., Danicke, S., Walk, N., Post, A., Kahlert, S., Rothkotter, H. J., and Kluess, J. (2011) Vulnerability of polarised intestinal porcine epithelial cells to mycotoxin deoxynivalenol depends on the route of application. *PLoS One* **6,** e17472
13. Pinton, P., Nougayrede, J. P., Del Rio, J. C., Moreno, C., Marin, D. E., Ferrier, L., Bracarense, A. P., Kolf-Clauw, M., and Oswald, I. P. (2009) The food contaminant deoxynivalenol, decreases intestinal barrier permeability and reduces claudin expression. *Toxicol. Appl. Pharmacol.* **237,** 41–48
14. Sergent, T., Parys, M., Garsou, S., Pussemier, L., Schneider, Y. J., and Larondelle, Y. (2006) Deoxynivalenol transport across human intestinal Caco-2 cells and its effects on cellular metabolism at realistic intestinal concentrations. *Toxicol. Lett.* **164,** 167–176
15. Pestka, J. J. (2010) Deoxynivalenol: mechanisms of action, human exposure, and toxicological relevance. *Arch. Toxicol.* **84,** 663–679
16. Pinton, P., Braicu, C., Nougayrede, J. P., Laffitte, J., Taranu, I., and Oswald, I. P. (2010) Deoxynivalenol impairs porcine intestinal barrier function and decreases the protein expression of claudin-4 through a mitogen-activated protein kinase-dependent mechanism. *J. Nutr.* **140,** 1956–1962
17. Pinton, P., Tsybulskyy, D., Lucioli, J., Laffitte, J., Callu, P., Lyazhri, F., Grosjean, F., Bracarense, A. P., Kolf-Clauw, M., and Oswald, I. P. (2012) Toxicity of deoxynivalenol and its acetylated derivatives on the intestine: differential effects on morphology, barrier function, tight junction proteins, and mitogen-activated protein kinases. *Toxicol. Sci.* **130,** 180–190
18. Sarkanj, B., Warth, B., Uhlig, S., Abia, W. A., Sulyok, M., Klapec, T., Krska, R., and Banjari, I. (2013) Urinary analysis reveals high deoxynivalenol exposure in pregnant women from Croatia. *Food Chem. Toxicol.* **62,** 231–237
19. Warth, B., Sulyok, M., Fruhmann, P., Berthiller, F., Schuhmacher, R., Hametner, C., Adam, G., Frohlich, J., and Krska, R. (2012) Assessment of human deoxynivalenol exposure using an LC-MS/MS based biomarker method. *Toxicol. Lett.* **211,** 85–90
20. Turner, P. C., Ji, B. T., Shu, X. O., Zheng, W., Chow, W. H., Gao, Y. T., and Hardie, L. J. (2011) A biomarker survey of urinary deoxynivalenol in China: the Shanghai Women's Health Study. *Food Addit. Contam. A* **28,** 1220–1223
21. Hepworth, S. J., Hardie, L. J., Fraser, L. K., Burley, V. J., Mijal, R. S., Wild, C. P., Azad, R., McKinney, P. A., and Turner, P. C. (2012) Deoxynivalenol exposure assessment in a cohort of pregnant women from Bradford, UK. *Food Addit. Contam. A* **29,** 269–276
22. Abassi, Y. A., Xi, B., Zhang, W., Ye, P., Kirstein, S. L., Gaylord, M. R., Feinstein, S. C., Wang, X., and Xu, X. (2009) Kinetic cell-based morphological screening: prediction of mechanism of compound action and off-target effects. *Chem. Biol.* **16,** 712–723
23. Sun, M., Fu, H., Cheng, H., Cao, Q., Zhao, Y., Mou, X., Zhang, X., Liu, X., and Ke, Y. (2012) A dynamic real-time method for monitoring epithelial barrier function in vitro. *Anal. Biochem.* **425,** 96–103
24. Kirkland, S. C. (1985) Dome formation by a human colonic adenocarcinoma cell line (HCA-7). *Cancer Res.* **45,** 3790–3795
25. Urcan, E., Haertel, U., Styllou, M., Hickel, R., Scherthan, H., and Reichl, F. X. (2010) Real-time xCELLigence impedance analysis of the cytotoxicity of dental composite components on human gingival fibroblasts. *Dent. Mater.* **26,** 51–58
26. Reeves, P. G. (1997) Components of the AIN-93 diets as improvements in the AIN-76A diet. *J. Nutr.* **127,** 838S–841S
27. Dombrink-Kurtzman, M. A., Poling, S. M., and Kendra, D. F. (2010) Determination of deoxynivalenol in infant cereal by immunoaffinity column cleanup and high-pressure liquid chromatography-UV detection. *J. Food Protect.* **73,** 1073–1076
28. Azcona-Olivera, J. I., Ouyang, Y., Murtha, J., Chu, F. S., and Pestka, J. J. (1995) Induction of cytokine mRNAs in mice after oral exposure to the trichothecene vomitoxin (deoxynivalenol): relationship to toxin distribution and protein synthesis inhibition. *Toxicol. Appl. Pharmacol.* **133,** 109–120
29. Moolenbeek, C., and Ruitenberg, E. J. (1981) The "Swiss roll": a simple technique for histological studies of the rodent intestine. *Lab. Anim.* **15,** 57–59

30. Danicke, S., Valenta, H., and Doll, S. (2004) On the toxicokinetics and the metabolism of deoxynivalenol (DON) in the pig. *Arch. Anim. Nutr.* **58,** 169–180

31. Videmann, B., Tep, J., Cavret, S., and Lecoeur, S. (2007) Epithelial transport of deoxynivalenol: involvement of human P-glycoprotein (ABCB1) and multidrug resistance-associated protein 2 (ABCC2). *Food Chem. Toxicol.* **45,** 1938–1947

32. Pestka, J. J. (2010) Deoxynivalenol-induced proinflammatory gene expression: mechanisms and pathological sequelae. *Toxins* **2,** 1300–1317

33. He, K., Zhou, H. R., and Pestka, J. J. (2012) Mechanisms for ribotoxin-induced ribosomal RNA cleavage. *Toxicol. Appl. Pharmacol.* **265,** 10–18

34. Kasuga, F., Hara-Kudo, Y., Saito, N., Kumagai, S., and Sugita-Konishi, Y. (1998) In vitro effect of deoxynivalenol on the differentiation of human colonic cell lines Caco-2 and T84. *Mycopathologia* **142,** 161–167

35. Yu, P., and Martin, C. M. (2000) Increased gut permeability and bacterial translocation in Pseudomonas pneumonia-induced sepsis. *Crit. Care Med.* **28,** 2573–2577

36. Wu, X., Vallance, B. A., Boyer, L., Bergstrom, K. S., Walker, J., Madsen, K., O'Kusky, J. R., Buchan, A. M., and Jacobson, K. (2008) Saccharomyces boulardii ameliorates Citrobacter rodentium-induced colitis through actions on bacterial virulence factors. *Am. J. Physiol. Gastrointest. Liver Physiol.* **294,** G295–G306

37. Hartsock, A., and Nelson, W. J. (2008) Adherens and tight junctions: structure, function and connections to the actin cytoskeleton. *Biochim. Biophys. Acta* **1778,** 660–669

38. Canil, C., Rosenshine, I., Ruschkowski, S., Donnenberg, M. S., Kaper, J. B., and Finlay, B. B. (1993) Enteropathogenic Escherichia coli decreases the transepithelial electrical resistance of polarized epithelial monolayers. *Infect. Immun.* **61,** 2755–2762

39. McLaughlin, J., Padfield, P. J., Burt, J. P., and O'Neill, C. A. (2004) Ochratoxin A increases permeability through tight junctions by removal of specific claudin isoforms. *Am. J. Physiol. Cell Physiol.* **287,** C1412–C1417

40. Mutch, D. M., Anderle, P., Fiaux, M., Mansourian, R., Vidal, K., Wahli, W., Williamson, G., and Roberts, M. A. (2004) Regional variations in ABC transporter expression along the mouse intestinal tract. *Physiol. Genomics* **17,** 11–20

41. Prelusky, D. B., Hartin, K. E., Trenholm, H. L., and Miller, J. D. (1988) Pharmacokinetic fate of 14C-labeled deoxynivalenol in swine. *Fund. Appl. Toxicol.* **10,** 276–286

42. Matsuda, M., Kubo, A., Furuse, M., and Tsukita, S. (2004) A peculiar internalization of claudins, tight junction-specific adhesion molecules, during the intercellular movement of epithelial cells. *J. Cell Sci.* **117,** 1247–1257

43. Zeissig, S., Burgel, N., Gunzel, D., Richter, J., Mankertz, J., Wahnschaffe, U., Kroesen, A. J., Zeitz, M., Fromm, M., and Schulzke, J. D. (2007) Changes in expression and distribution of claudin 2, 5 and 8 lead to discontinuous tight junctions and barrier dysfunction in active Crohn's disease. *Gut* **56,** 61–72

44. Bruewer, M., Utech, M., Ivanov, A. I., Hopkins, A. M., Parkos, C. A., and Nusrat, A. (2005) Interferon-gamma induces internalization of epithelial tight junction proteins via a macropinocytosis-like process. *FASEB J.* **19,** 923–933

45. Ivanov, A. I., Nusrat, A., and Parkos, C. A. (2004) The epithelium in inflammatory bowel disease: potential role of endocytosis of junctional proteins in barrier disruption. *Novartis Found. Symp.* **263,** 115–124; discussion 124–132, 211–118

46. Prasad, S., Mingrino, R., Kaukinen, K., Hayes, K. L., Powell, R. M., MacDonald, T. T., and Collins, J. E. (2005) Inflammatory processes have differential effects on claudins 2, 3 and 4 in colonic epithelial cells. *Lab. Invest.* **85,** 1139–1162

47. Rahner, C., Mitic, L. L., and Anderson, J. M. (2001) Heterogeneity in expression and subcellular localization of claudins 2, 3, 4, and 5 in the rat liver, pancreas, and gut. *Gastroenterology* **120,** 411–422

48. Tamagawa, H., Takahashi, I., Furuse, M., Yoshitake-Kitano, Y., Tsukita, S., Ito, T., Matsuda, H., and Kiyono, H. (2003) Characterisics of claudin expression in follicle-associated epithelium of Peyer's patches: preferential localization of claudin-4 at the apex of the dome region. *Lab. Invest.* **83,** 1045–1053

49. Fujita, H., Chiba, H., Yokozaki, H., Sakai, N., Sugimoto, K., Wada, T., Kojima, T., Yamashita, T., and Sawada, N. (2006) Differential expression and subcellular localization of claudin-7, -8, -12, -13, and -15 along the mouse intestine. *J. Histochem. Cytochem.* **54,** 933–944

50. Will, C., Fromm, M., and Muller, D. (2008) Claudin tight junction proteins: novel aspects in paracellular transport. *Perit. Dial. Int.* **28,** 577–584

51. Fujita, K., Katahira, J., Horiguchi, Y., Sonoda, N., Furuse, M., and Tsukita, S. (2000) Clostridium perfringens enterotoxin binds to the second extracellular loop of claudin-3, a tight junction integral membrane protein. *FEBS Lett.* **476,** 258–261

52. Suzuki, T. (2013) Regulation of intestinal epithelial permeability by tight junctions. *Cell. Mol. Life Sci.* **70,** 631–659

53. Kolf-Clauw, M., Castellote, J., Joly, B., Bourges-Abella, N., Raymond-Letron, I., Pinton, P., and Oswald, I. P. (2009) Development of a pig jejunal explant culture for studying the gastrointestinal toxicity of the mycotoxin deoxynivalenol: histopathological analysis. *Toxicol. In Vitro* **23,** 1580–1584

54. Blikslager, A. T., Moeser, A. J., Gookin, J. L., Jones, S. L., and Odle, J. (2007) Restoration of barrier function in injured intestinal mucosa. *Physiol. Rev.* **87,** 545–564